# On the working process theory of high temperature jet and turbojet engines in experimental achivements light of modern physics

*M.J. Ivanov, V.K. Mamaev, G. B. Zhestkov*

*Central Institute of Aviation Motors (CIAM)*
*Moscow, 111116, Aviavotornaya St., 2 Russia*

## Abstract

Simulation of complex working processes of jet and turbojet engine different types is considered. The first part of the paper presents the gas dynamics model for whole engine, detail simulation of radiation component, the close systems of thermodynamically compatible conservation laws and typical results for a turbojet engine modeling. The second part of the paper demonstrates a few experimental results of modern physics and astrophysics, which are important for high temperature engine theory development. We show solutions for cosmic jet engines and gamma-ray bursts. Achievements in experimental physics and nanotechnologies pointed out also that it would be useful additionally to modification of high temperature gas turbine theory.

## 1. Introduction

Working process theory of high temperature jet and turbojet engines demands accurate simulation for each component, including heat addition and radiation losses in combustors and turbine. Well known experience of V generation engine creation has pointed out the imperfection of modern thermodynamic working process models. The theoretically calculated in design stage engine parameters essentially differ from experimental data for first engine units. Hence, long and expensive development of new high temperature jet and gas turbine engines is required. The typical examples there are presented in [1-3].

We consider simulation of complex working processes of jet and turbojet engine different types [4]. Here the paper present the gas dynamics model for whole engine passage, the radiation component modeling, the close systems of thermodynamically compatible conservation laws and typical results for a turbojet engine simulation [5].

The paper demonstrates also a few experimental achievements of modern physics and astrophysics, which are important for high temperature engine theory development. Registration of cosmic microwave background radiation is among such achievements. The results of conducted researches indicated that frequency distribution of background radiation density corresponds to frequency distribution of radiation density from the black body with its temperature T=2.725 K (near 3 K). The second significant achievement is the discovery of Dark Matter (DM), which is also called “the hidden mass in the Universe”[6-10]. Now we know that 96% whole matter in our Universe consists of DM. The baryonic substance accounts to only 4%. There were multiple attempts to describe the nature of DM, but none was successful yet (see, in particular, [6]). The third important success is the discovery of vacuum polarization around electrons, protons and atomic centers. Intensive light impulse propagation leads to creation of electron-positron pair at the collision of two powerful electromagnetic pulses. Possibility to determine the shape of separate atoms and molecules via scanning probe microscopy is the fourth important for us achievement of experimental physics. It became possible to see so called van der Waals spheres and real polarized space around atomic centers [10].

Using emphasized achievements the more accurate simulation for nuclear, atomic and molecule structures have been considered in our paper. The equation for description of electrical potential distribution in polarized space is provided. We analyze the specific solution in polarized space of electron and proton with the presence of some barriers, which allow electrons to be on corresponding orbits of atom in stationary states. We propose the method of STationary Electrons (STEL) for atomic and molecule structures description. This model provides very forming via the linkage of stationary electrons on outer atomic orbits. Such spatial molecular structures are fully according to widely accepted physics and chemistry conception [10]. We present also calculation results for nucleus internal structure of deuterium, tritium and helium $^{3}$He and $^{4}$He.

The work contains a lot of practical applications for GTE flow path designing with the use of considered approaches. The results of such calculations practically coincide with experimental data and parameters of already realized GT engine projects [11, 12].

## 2. Simulation of steady and unsteady flows in whole gas turbine engine

Unsteady processes in whole engine flow passage (fig. 1) are simulated using unsteady approach based on Euler or Navier-Stokes equations. Detailed formulations of the used approach can be found in [11, 12]. The brief description of this method is provided in this article.

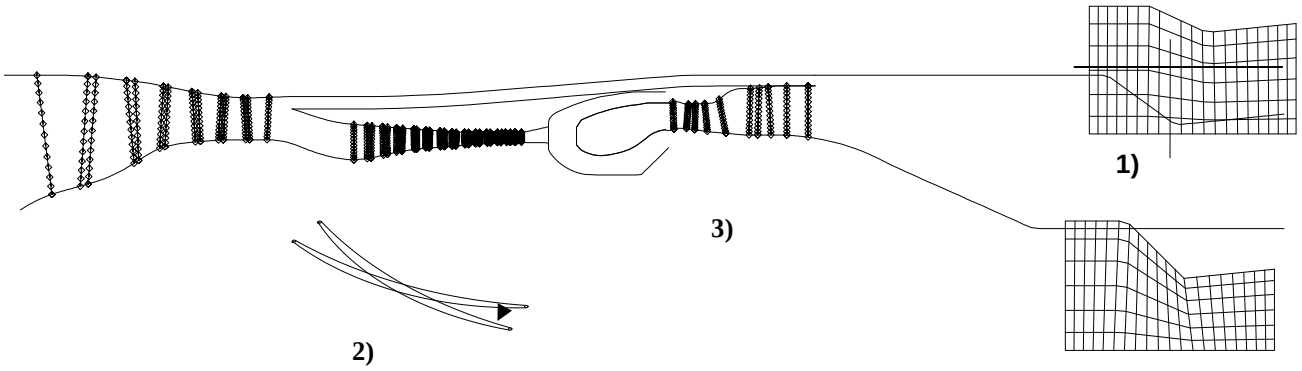


Figure 1: Engine management scheme with variable elements:
1) exhaust nozzle; 2) stagger angle of vane; 3) thermal expansion, etc.

The governing equations can be derived from 3D equations written in conservative form for special body fitted curvilinear coordinates:

$$
\begin{aligned}
&\xi = \xi(z, r, \varphi), \eta = \eta(z, r, \varphi), \zeta = \zeta(z, r, \varphi);\\
&\frac{\partial}{\partial t}\left(\frac{r\bar{U}}{J}\right) + \frac{\partial}{\partial \xi}\left(\frac{r}{J}\left(\bar{F}\xi_z + \bar{G}\xi_r + \bar{H}\frac{1}{r}\xi_\varphi\right)\right) +\\
&+ \frac{\partial}{\partial \eta}\left(\frac{r}{J}\left(\bar{F}\mu_z + \bar{G}\eta_r + \bar{H}\frac{1}{r}\eta_\varphi\right)\right) +\\
&+ \frac{\partial}{\partial \zeta}\left(\frac{r}{J}\left(\bar{F}\zeta_z + \bar{G}\zeta_r + \bar{H}\frac{1}{r}\zeta_\varphi\right)\right) = \frac{\bar{h}}{J},\\
&\mathrm{J} = \frac{\partial(\zeta, \eta.\zeta)}{\partial(z, r, \varphi)},
\end{aligned}
\tag{1}
$$

where $J$ – Jacobian of the coordinate transformation, $\xi_z, \xi_r, \ldots$ - the transformation coefficients (partial derivatives).

In axisymmetrical domains the final equations can be written in the form:

$$
\begin{aligned}
&\zeta = \varphi, \quad \xi_\varphi = \eta_\varphi = 0, \quad \frac{\partial}{\partial \zeta} = 0\\
&\frac{\partial}{\partial t}\left(\frac{r\bar{U}}{J}\right) + \frac{\partial}{\partial \xi}\left(\frac{r}{J}(\bar{F}\xi_z + \bar{G}\xi_r)\right) +\\
&+ \frac{\partial}{\partial \eta}\left(\frac{r}{J}(\bar{F}\eta_z + \bar{G}\eta_r)\right) = \frac{\bar{h}}{J}
\end{aligned}
\tag{2}
$$

In the bladed domains a special so-called S2 surface is considered, and the governing equations are written in the form:

$$\begin{cases} \xi_z\zeta_z + \xi_r\zeta_r + \dfrac{1}{r^2}\xi_\varphi\zeta_\varphi = 0, \\ \eta_z\zeta_z + \eta_r\zeta_r + \dfrac{1}{r^2}\eta_\varphi\zeta_\varphi = 0. \end{cases}; \quad \begin{array}{l} \dfrac{\partial}{\partial t}\left(\dfrac{r\bar{U}}{J}\right) + \dfrac{\partial}{\partial \xi}\left(\dfrac{r}{J}\left(\bar{F}\xi_z + \bar{G}\xi_r + \bar{H}\dfrac{1}{r}\xi_\varphi\right)\right) + \\ + \dfrac{\partial}{\partial \eta}\left(\dfrac{r}{J}\left(\bar{F}\eta_z + \bar{G}\eta_r + \bar{H}\dfrac{1}{r}\eta_\varphi\right)\right) = \dfrac{\bar{h}}{J} + \bar{h}_1 \end{array} \tag{3}$$

First two equations are algebraic constraint equations. The governing equations are written in conservative form and thus can be used in the cases when strong discontinuities and other transonic effects take place in the flow field.

In addition to the system (3) the next rotor motion equations should be used:

$$J_j^0 \frac{d\omega_j}{dt} = M_j^T - M_j^C - M_j^f, \tag{4}$$

where $J_j^0$ - moment of inertia of rotor, numbered *j*, $M_j^T, M_j^C, M_j^f$ - torque of turbine, compressor and friction (or other additional torque) correspondingly for the rotor number *j*.

Mathematical formulation of the problem is closed by the state equations, which are written in the next form for the general case of gas-air mixture:

$$\begin{aligned} & p = \rho RT \sum_{i=1}^{N} \frac{c_i}{\mu_i}, \\ & \mathrm{e} = \rho\left[\mathrm{h} + \frac{1}{2}(u^2 + v^2 + w^2)\right] - p, \\ & h = \sum_{i=1}^{N} c_i h_i(T), \\ & \mathrm{h_i}(T) = \int_{T_0}^{T} c_{p_i}(\tau)d\tau + h_{0i}, \quad \mathrm{c_{p_i}}(\tau) > 0 \end{aligned} \tag{5}$$

*T* herein is an absolute temperature, $c_i$ - mass concentrations of the mixture components, $\mu_i$ - molecular weight of the *i*-component. Mass concentrations of the working media are changed mainly only in combustion chambers, where chemical composition is changed due to the combustion processes, and in cooled turbines, where cooling air is blowing out into the main working gas flow passage.

To allow for variable elements in engines the next approach is used in the considered mathematical model. A quantity of base numerical grids is generated for each domain containing the variable elements (Fig. 1), each grid corresponds to possible geometry conditions. The base grids should cover all considered range of the geometry variation and should have identical topology and dimension. A parameter value is associated with each of the grids. For example, stagger angle for the variable guide vane or the throat area for the nozzle. For each time moment (or for each iteration) the current grid of the domain is found by the interpolation from the base grids using the current values of the associated parameters (for example, using the value of the corrected HP spool speed).

High order accuracy conservative and monotone numerical scheme based on the Godunov's scheme is used to solve the equations system.

In the 3D approach the initial 3D governing equations (1) are solved. Algebraic and two-equation (q-ω) model were used for the turbulence simulation.

### 3. The correlation of HPT parameters in GTE system

In his series of articles known as "Air-breathing engines theory" (1947) B.S. Stechkin paid a lot of attention to problems of air-gas channel losses evaluation. He thoroughly analyzed the generic diagram of GTE physical cycle with increased losses in intensive heat application conditions (see [13], fig.49, page 109).

Segment 2-3 of fig.2 corresponds the heat application process. It ends at point 3 (point 3' corresponds the end of ideal process) of line $T_3^* = const$. The full pressure correlation can be written as follows

$$\sigma_{c.c.} p_2^* = p_{3g}^* + p_{3r}^*, \tag{6}$$

Component $p_{3r}^*$ corresponds additional heat effects (fig.2).

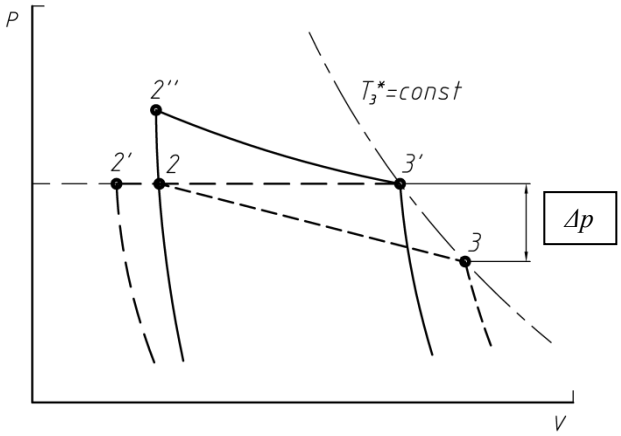


Figure 2: Heat application, $\Delta p$ - thermal losses

This form of logging should be explained. In high temperature conditions of flame tubes the heat radiation takes place. It is shielded by walls of combustion chambers. These radiation effects increase the pressure of working medium in flame tubes. Therefore the right part of equation (6) is expressed via sum of working medium pressure $p_{3g}^*$ and additional $p_{3r}^*$, caused by heat radiation. The analysis of available experimental data allows to evaluate $p_{3r}^*$, which is defined by $T_3^*$ (at $T_3^* \approx 1500$ K $p_{3r}^*$ accounts 5-7% of total pressure).

The mechanical work on the GTE shaft is committed by the cost of $p^*{}_{3g}$ component decrease. Whereas the heat radiation component leads to additional heating of flame tube and HPT surfaces. However some percentage of this energy is returned to the working medium. Analysis of modern GTE allows to obtain quantitative characteristic of working process.

The correlation of engine via equation (1) is more accurate than the correlation with the aid of traditional equation. In his design calculation Stechkin increased the air compression by 7-8% in comparison with traditional way of engine correlation. Thus the design parameters at the turbine inlet were obtained (see line 2''-3' in fig.2). This method greatly economized time.

It should be noted that the correlation (6) is valid only in conditions of thermodynamic equilibrium between gaseous working medium with high temperature $T_3^*$ and heat radiation with the same equilibrium temperature value. The flow velocity in main GTE combustion chambers is low (Mach number usually doesn't exceed 0.05-0.08) and the gas particles have time for energy exchange with radiation (thermodynamic equilibrium condition is achieved).

Heat radiation effect can be modeled via improved state equation

$$\frac{p}{\rho RT} = 1 + \rho B(T), \tag{7}$$

Virial coefficient B(T) corresponds the heat radiation pressure. Its approximate value can be obtained from experimental data of high temperature GTE correlation. Equation (7) has local character (defines pressure value in local spot of flow), while equation (6) has integral character (defines values in turbine inlet section). Both these equations were written according to identical assumptions about the significant influence of heat radiation upon heat application process.

## 4. Gas dynamic model of radiation component

We present the gas dynamic model of radiation component, which bases on a classic empirical radiation data and some modern physics experimental results. For detail analysis it will be enough to use the four based initial premises: 1) The radiation component is the same as classic gaseous medium with the adiabatic constant $\kappa=4/3$ (similar as photon gas with non-zero mass of particles). 2) The stream of equilibrium radiation $S$ with a black body surface determines by the Stephan – Boltzmann's law $S=\sigma T^4$ Wt/m$^2$, where $\sigma=5.67\cdot10^{-8}$ Wt/m$^2$/K$^4$. 3) Initial temperature of radiation component near the Earth equals the background microwave radiation temperature $T_0$=2.735 K. 4) The velocity of weak perturbation propagation in compressible radiation medium with temperature $T_0$=2.735 K is the light velocity in vacuum $c=3\cdot10^8$ m/s.

Presented four premises allow formulating the full enough physical and mathematical model for the radiation component. Summarized of our premises we can emphasize that a considered in this paper radiation component is the traditional photon gas (with $\kappa=4/3$) and the classic ether (a compressible gas with non-zero mass of particles). Using the simple enough gas kinetic theory we can determine a mass $m$ of gas particle. Average kinetic energy is

$$E = \frac{mv_{av}^2}{2} = \frac{3}{2}kT_0 = m\frac{3}{2}\frac{R_u T_0}{mN} =$$
$$= \frac{m}{\kappa}\frac{3}{2}\kappa\frac{p_0}{\rho_0} = \frac{9}{8}mc^2.$$

Here $k = R_u / N$ - the Boltzmann's constant, $R_u$ – a universe gas constant, $N$ – the Avogadro's number. Therefore we calculate

$$m = \frac{4}{3}\frac{kT_0}{c^2} = 5.6\cdot 10^{-40} \text{ kg.}$$

The gas constant $R = R_u / mN$ and the specific heat $c_v$ and $c_p$ can be found from

$$R = \frac{k}{m} = 0.25\cdot 10^{17} \text{ J/kg·K,}$$
$$c_v = 0.75\cdot 10^{17} \text{ J/kg·K, } c_p = R + c_v = 1\cdot 10^{17} \text{ J/kg·K.}$$

Remembering the first premise for the radiation component we have the traditional state equation

$$p = \rho RT,$$

which can be written as

$$p = (\kappa - 1)\rho e,$$

where $e = c_v T$ - specific internal energy.

From the second and the third laws of thermodynamics we can estimate initial pressure $p_0$ and density $\rho_0$ for a radiation component by the initial temperature $T_0$=2.735 K. For steady volume $\Omega$ with boundary $\Gamma$ the energy low is written

$$\frac{\partial}{\partial t}\iiint_{\Omega} \rho e d\omega = -\iint_{\Gamma} \bar{S}\cdot\bar{n}d\gamma$$

or in differential form

$$\frac{\partial \rho e}{\partial t} = -div\bar{S}.$$

We integrate this equation for the 1D case from the initial data with $T$=0 and $p$=0 to data $T_0$=2.735 K and $p_0$, when for unit volume with $T$=0 on the left and $T = T_0$ on the right boundaries and obtain

$$\rho_0 e_0 = \frac{p_0 D}{\kappa - 1} = \sigma T_0^4,$$

where $D = \Delta x / \Delta t$. For the case with $D$=1 we have

$$p_0 = (\kappa - 1)\sigma T_0^4 = 10^{-6} \text{ Pa, } \rho_0 = p_0 / RT_0 = 1.46\cdot 10^{-23} \text{ kg/m}^3.$$

The presented values $p_0$, $\rho_0$ and $T_0$ show the radiation component parameters in vacuum. Also, for adiabatic process in a radiation medium one may be obtained

$$\frac{p}{p_0} = \left(\frac{T}{T_0}\right)^{\frac{\kappa}{\kappa-1}}.$$

The adiabatic compression to temperature $T$=1500 K, 1700 K, 1900 K and 2100 K gives $p$=1, 1.5, 2.3 and 3.5 atmospheres. These addition pressures should include into account in the practice applications.

**5. Conservation laws for one velocity two components model with gas and radiation components.**

Now we present the common conservation laws system for one velocity two components model of a gaseous medium with detail description of radiation effects. It will be used the index *g* for a gas and the index *f* for a radiation components of medium (for example, for densities $\rho_g$ and $\rho_f$) and without index for summarize value ($\rho=\rho_g+\rho_f$). For the one velocity model the values of velocity $\bar{V}$ and their components *u,v,w* on the axis *x,y,z* are the same for each medium components.
The mass conservation laws are

$$\frac{\partial \rho_g}{\partial t} + div(\rho_g \bar{V}) = q_g,$$
$$\frac{\partial \rho_f}{\partial t} + div(\rho_f \bar{V}) = q_f.$$

The summary law we obtain as composition of this two equations

$$\frac{\partial \rho}{\partial t} + div(\rho \bar{V}) = q,$$

where $\rho = \rho_g + \rho_f$, $q = q_g + q_f$ - souse terms.
The impulse conservation laws

$$\frac{\partial \rho_g \bar{V}}{\partial t} + div(\rho_g \bar{V}(\bar{V} \cdot \bar{n})) + grad\ p_g = r_f$$

$$\frac{\partial \rho_f \bar{V}}{\partial t} + div(\rho_f \bar{V}(\bar{V} \cdot \bar{n})) + grad\ p_f = r_f$$

and the summary law

$$\frac{\partial \rho \bar{V}}{\partial t} + div(\rho \bar{V} \cdot (\bar{V} \cdot n)) + grad\ p = r$$

where $p = p_\rho + p_f$, $r = r_\rho + r_f$.
The energy conservation laws

$$\frac{\partial \rho_g e_g}{\partial t} + div(\rho_g e_g \bar{V}) + p_g div\bar{V} =$$
$$= div(K_g grad T_g) + c_{fg}(T_f - T_g) + Q_g,$$

$$\frac{\partial \rho_f e_f}{\partial t} + div(\rho_f e_f \bar{V}) + p_f div\bar{V} =$$
$$= div(K_f grad T_f) + c_{fg}(T_g - T_f) + Q_f$$

and the summary law

$$\frac{\partial \rho e}{\partial t} + div(\rho e \bar{V}) + p\, div\bar{V} = -divW + Q,$$

where

$$e = \frac{\rho_g}{\rho} e_g + \frac{\rho_f}{\rho} e_f,\ -W = K_g grad T_g + K_f grad T_f,$$
$$Q = Q_g + Q_f.$$

Energy conservation laws are written for heat transfer gas and radiation components (the first terms in the right side of these equations, $K_g$ and $K_f$ correspondently thermo transfer coefficients for gas and radiation parts). The second terms in the right side describe a energy exchange between gas and radiation parts. The last terms $Q_g$ and

$Q_f$ are an additional energy souses, which include into account energy exchange channels (for example, in the case chemical reactions).
The energy conservation laws can be written in the form

$$\frac{\partial \rho\left(e+\frac{V^2}{2}\right)}{\partial t}+div\left[\left(\rho(e+\frac{V^2}{2})+p\right)\bar{V}\right]=-divW+Q\,.$$

The high level of gas turbine working process models [11] based on this system allow to get accurate simulation of thermodynamic process for high temperature gas turbine engines. The paper presents typical results of this model application.

### 6. Turbojet engine working process simulation

The typical flow passage of aviation gas turbine engine in meridional plane (z, r) is shown in fig. 1. The main parts of engine (here it is a turbojet bypass engine with afterburner) are: fan (low pressure compressor), high pressure compressor (with a few variable guide vanes), main angular combustor chamber, high pressure turbine, low pressure turbine, afterburner, secondary contour, variable-area nozzle. A simulation of working fluid (air or gas) moving is fulfilled in the whole flow of engine including core and bypass duct. It seems to be convenient to use in this case fast enough 3D thin layer viscous approaches with wall functions for algebraic or differential turbulence models.

The described above approaches were used in the investigation of steady and unsteady working points of the bypass gas turbine engine (fig. 3–5). The engine was investigated in detail experimentally. Both the whole engine and the core engine were tested.

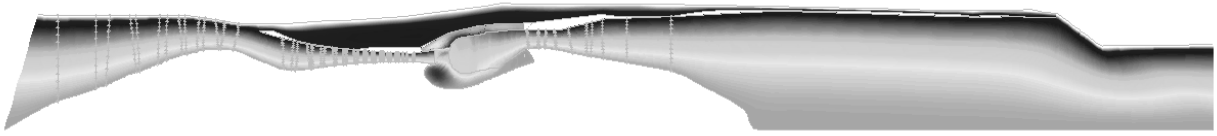

Mass flow distribution

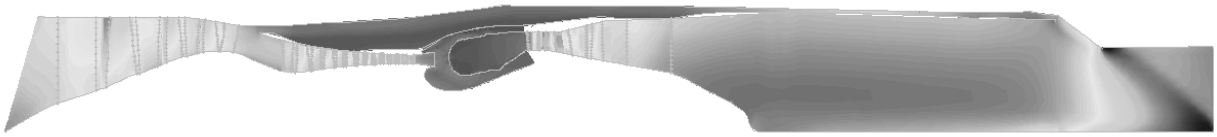

Mach number

Figure 3: Examples of steady and unsteady calculations

A mathematical model of the engine allowed variable elements as described above. Different design and off-design working points were studied and compared with the test results. The experiments demonstrated significant discrepancy between the tested and design engine parameters for a number of working points. In became apparent first of all in the decreased flow capacity of the compressor, and led finally to increased turbine inlet temperatures, decreasing thrust etc. (fig. 3-5).

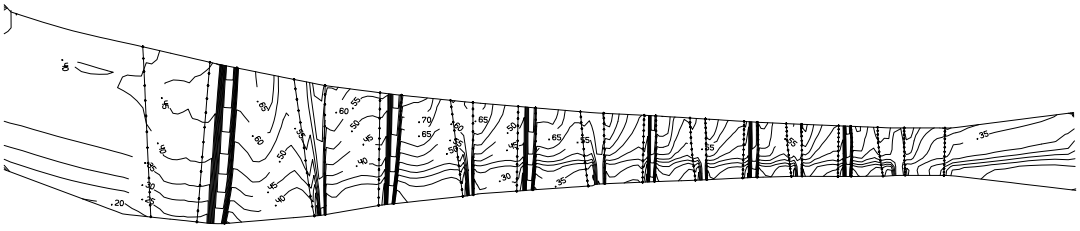

Figure 4: Mach number contours in the compressor part of flow passage.
The working point for 100% rotational speed.

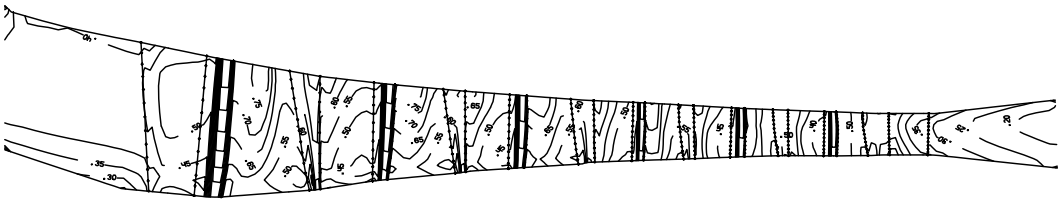

Figure 5: Mach number contours in the compressor part of flow passage
(stagger angle of vane +1.5°).

Channel flow with heat addition simulation is presented on fig. 6. We can see temperature and pressure distributions inside channel and on up and down walls.

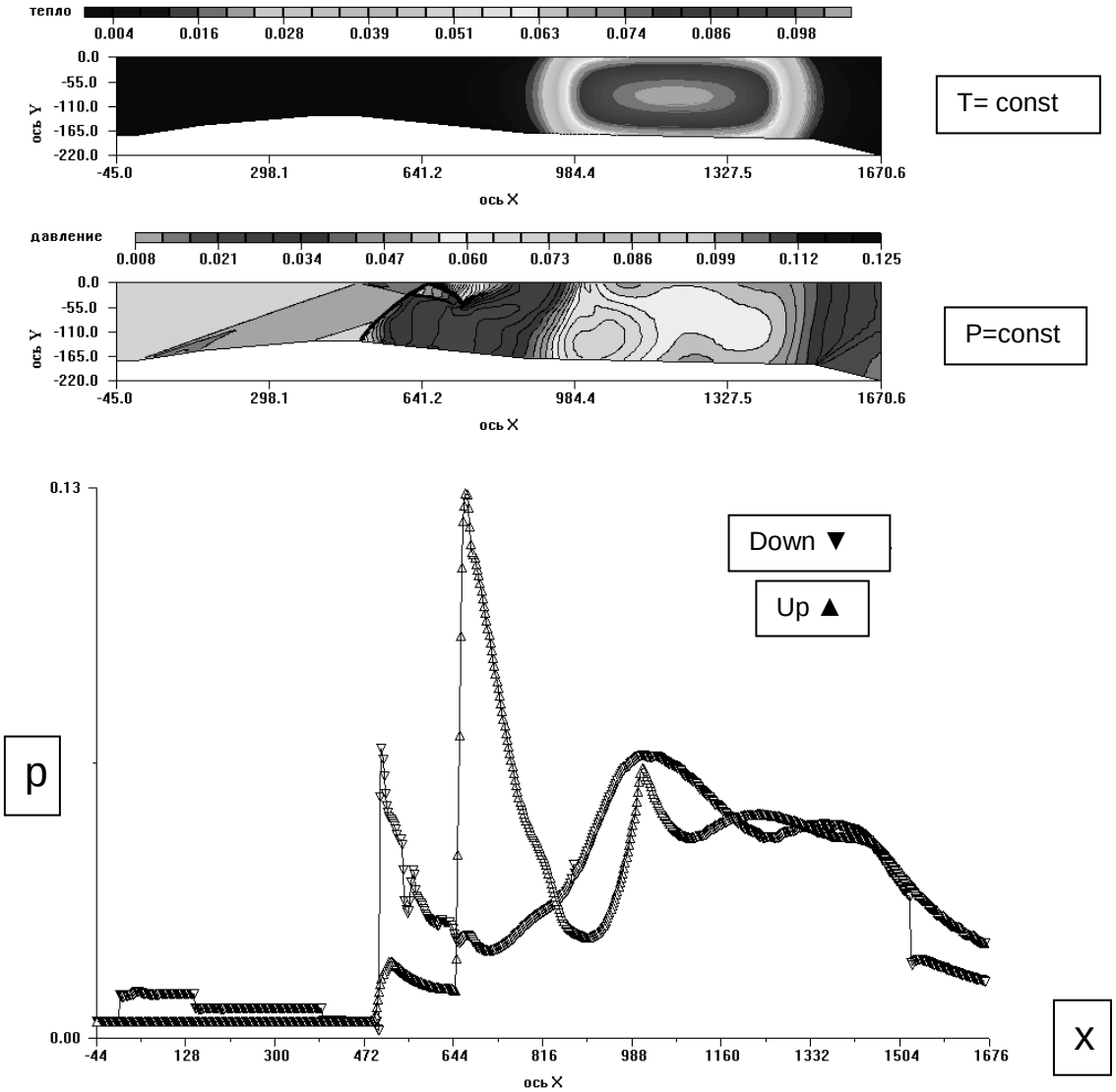


Figure 6: Wall pressure distributions in channel with intensive heat addition.

## 7. Physics applications of the modeling

Let's demonstrate now possible application of our modeling within the frame of classical mechanics approach of a number of mysterious astrophysics phenomena. A good theoretic model of gamma-bursts can be represented by the above considered superluminal soliton solutions of rather big amplitude, which move in the dark matter medium without changing their shapes and loss of energy. We also give calculated solutions of the decomposition task of initial contraction for sequence of soliton solutions (fig. 7). As a result of such decomposition a sequence solitons with decreasing amplitude and propagation velocity is formed. The similar solutions can simulate the effects of gamma-bursts after glowing, which later reaches an observer (with the delay of several years).

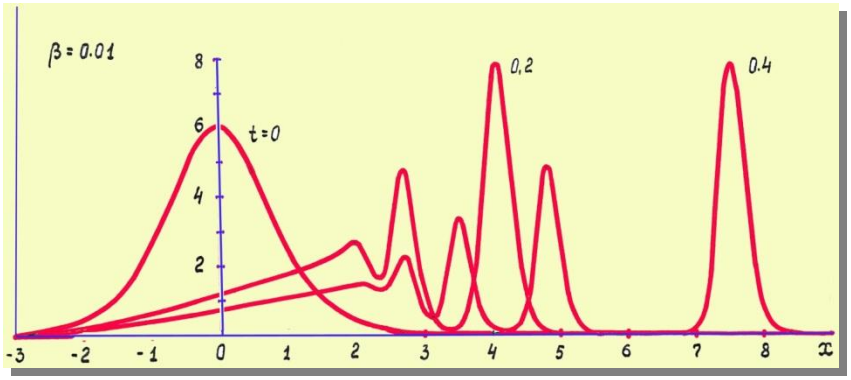


Figure 7. Gamma-ray burst propagation.

Fig. 8 displays a scheme of an active galaxy with two superluminal jets flowing from its center in opposite directions and the calculation results of several "barrels" of such extragalactic jets are given.

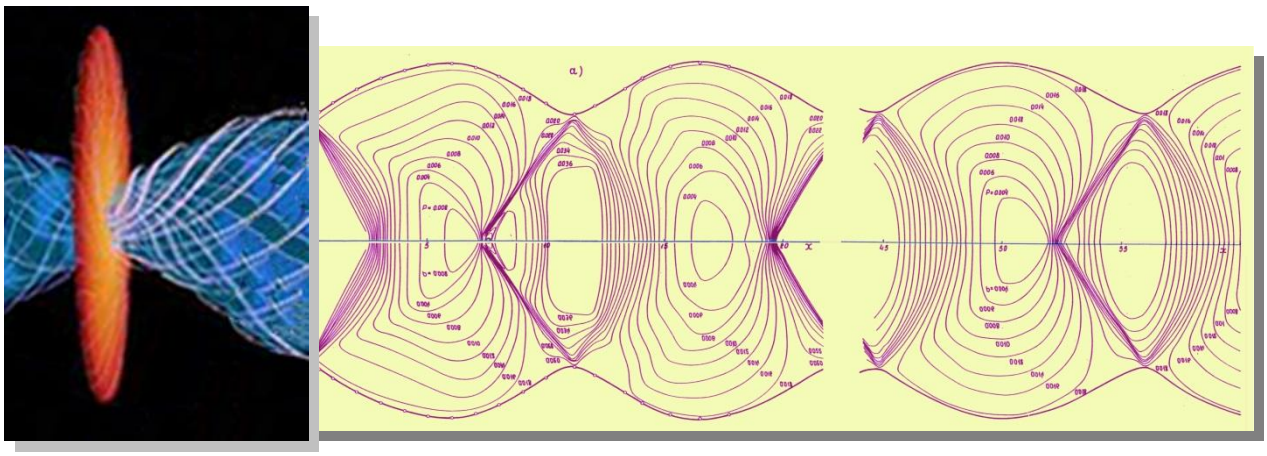

Figure 8: Natural jet engines (cosmic jet).

In the context of the present study, the possibilities of mechanical simulation for a few nucleus, atoms and molecules are considered. Based on the nature of gaseous Dark Matter (DM) the equation for electrical potential distribution is provided. This equation has been solved for cases of electron and proton polarized spaces. The obtained solutions show we the presence of some potential barriers on the boundaries of polarized spaces of a charge particles. That's why Thomson – Rutherford improved atomic model can be used, and we propose the method of STationary ELectrons (STEL) for atomic and molecule structures description. This model provides very graphic description of valence linkages (ionic, covalent, semi polar and oth.), which are forming via the linkage of stationary electrons on outer atomic orbits. Such spatial molecular structures are fully according to widely accepted physics and chemistry conception.

The STEL model of hydrogen linkages can be imagined in classical form when first envelope from proton occupied

by two electrons, which belong to two negative ions. For instance, ion of hydrogen difluoride $HF^{-}_{2}$ with linear structure $F^{-}H^{-}F^{-}$ is stable due to proton, which unites two negative ions via Coulomb interaction. Special consideration has fulfilled for hydrocarbon valence linkages in benzoyl $C_6H_6$ and naphthalene $C_{10}H_8$ molecules. We give the molecule images, their detail structures (fig. 9 and also electronic and structural formulas (fig. 10). It should be emphasized that the benzoyl ring has internal linkages between carbon atoms through three stationary electrons.

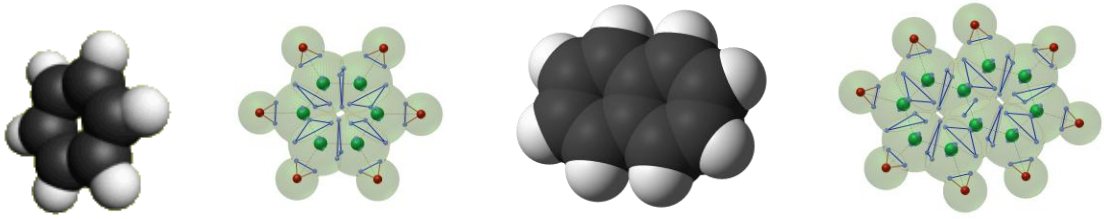

Figure 9: . Benzoyl $C_6H_6$ and naphthalene $C_{10}H_8$ molecules and their form.

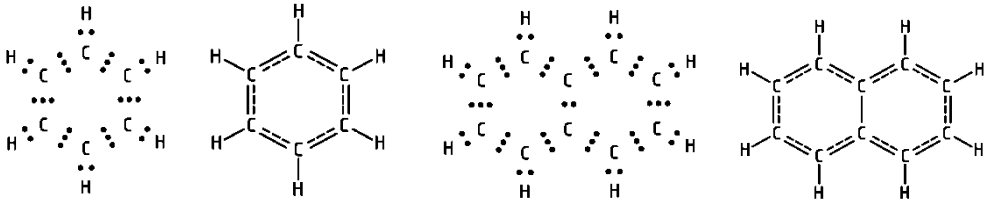

Figure 10: Electronic and structural formulas of benzoyl $C_6H_6$ and naphthalene $C_{10}H_8$ molecules.

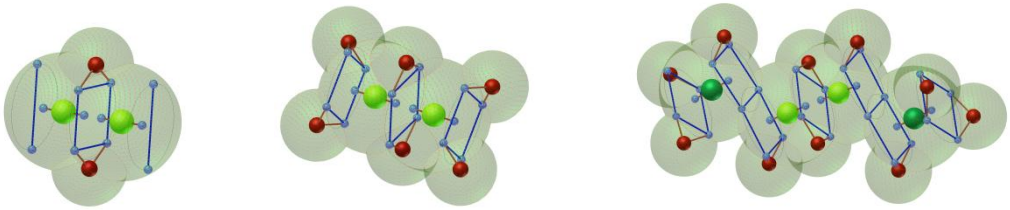

Figure 11: Complex $B_2H_2$ and molecules $B_2H_6$ and $B_4H_{10}$

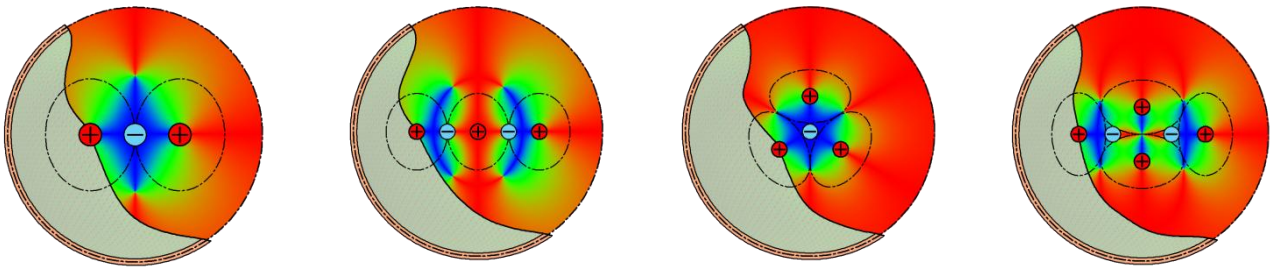

(a) (b) (c) (d)

Figure 12: Internal structures of deuterium (a), tritium (b) and helium $^{3}$He (c) and $^{4}$He (d).

The next examples are related to borohydrogen molecules $B_2H_2$, $B_6H_6$, $B_4H_{10}$ (fig. 11). The complex $B_2H_2$ has special type of internal four electrons linkage and outer four valence linkages, similar the carbon and silicon atoms. Also it is possible to describe metallic bonding from our deterministic position.

The STEL model allows us to simulate also an internal nuclear structures. Fig. 12 shows the typical nuclear structures for deuterium, tritium, helium $^{3}$He and $^{4}$He. It should be noted that the used CFD simulation shows also the possibility of mechanical description for any gaseous medium (including DM) with united modeling of strong, weak and electromagnetic interactions [10].

Achievements in experimental physics and nanotechnologies pointed out also that it would be useful additionally to modification of high temperature gas turbine theory.

**Acknowledgments**

Author thanks B. Muraviov for assistance.

**References**

[1] Aviation Week, 2012, Vol.174, No.29, p.17.
[2] Flight, 2012, Vol.181, No.5343, p.33.
[3] Flight, 2012, Vol.182, No.5351, p.19.
[4] Ivanov M.Ja**.,** Mamaev B.I., Nigmatullin R.Z. United Modeling of Working Process in Aircraft Gas Turbine Engines", *ASME Paper*, No. 50185, 2008, 10 p.
[5] Ivanov M.Ja**.** Thermodynamically compatible conservation laws in the model of heat conduction radiating gas. Comp. Math. and Math. Phys., 2011, Vol. 51, No. 1, pp. 133-142.
[6] Mavromatos N. Recent results from indirect and direct dark matter searches – Theoretical scenarios. 13th ICATPP Conference. Villa Olmo, Como 3-7 Oct. 2011. P.23
[7] Ivanov M.Ja., Zhestkov G.B. Dimensional Analysis, Thermodynamics and Conservation Laws in a Problem of Radiation Processes Simulation, *J. of Math. Research*, 2012, Vol. 4, No.2, pp. 10-19.
[8] Ivanov M.Ja., Mamaev V.K. Hidden Mass Boson. *J. Modern Physics*, 2012, Vol. 3, No. 8, pp. 686-693.
[9] Ivanov M.Ja Classic Dark Matter Theory with Experimental Confirmations, Exact Solutions and Practical Applications. Cosmology. 47-th Rencontres de Moriond, 10 – 17 March, 2012, La Thuile, Aosta valley, Italy.
[10] Ivanov M.Ja. "Space Energy," Energy Conservation, Ed. A.Z. Ahmed, INTECH, 2012, pp.3-56.
[11] Abzailov A.I., Ivanov M. Ja., Nigmatullin R.Z. Steady and transient working mode simulation for turbojet bypass engines based on meridional axisymmetric approach. 2005, ISABE 2005-1083, p.7.
[12] Ivanov M. Ja., Nigmatullin R. Z. The aerodynamics of GTE air-gas channel. CIAM, 2001-2005, The main results of scientific research, Moscow, 2005, pp. 80-84.
[13] Stechkin B.S., "Heat engine theory" 1977, Nauka publishing, Moscow.